Available online at www.sciencedirect.com
SCIENCE DIRECT®

ELSEVIER

Microelectronic Engineering 69 (2003) 519–527

MICROELECTRONIC ENGINEERING

www.elsevier.com/locate/mee

Nanoindentaion techniques for assessing mechanical reliability at the nanoscale

Alex A. Volinsky[a,*], William W. Gerberich[b]

[a]Process and Materials Characterization Laboratory, MD EL-622, Motorola Inc., 210 E. Elliot Road, Tempe, AZ 85284, USA
[b]Department of Chemical Engineering and Materials Science, University of Minnesota, Minneapolis, MN 55455, USA

Abstract

Nanoindetation is a powerful technique for measuring mechanical properties of thin films. First applied over 20 years ago in the hard drive industry, it is now commonly used for other applications. This paper describes nanoindentation techniques for measuring thin films mechanical properties, including elastic modulus, hardness, adhesion and fracture toughness as applied for modern microelectronics reliability. Elastic, plastic and adhesion properties of Cu interconnects are discussed, including the influence of film microstructure, thickness and grain size. Elastic, fracture and adhesion properties of advanced low-*K* dielectrics also discussed along with the current challenges of nanoindentation data interpretation and analysis as applied for advanced electronic materials.

Keywords: Nanoindentation; Mechanical reliability; Adhesion; Interconnects; Low-*K* dielectrics

1. Introduction

The rapid growth in the microelectronics industry for the past several years requires very fine interconnects with thin metal lines within one chip. A modern integrated circuit (IC) contains more than 200 million transistors. There is a need to increase the number of transistors while lowering the chip's dimensions and reducing the power consumption. Aluminum interconnects in the microelectronic devices have been pushed to their dimensional limits due to reliability (electromigration and stress migration) problems. Copper, having a higher conductivity and better electromigration properties is replacing aluminum in integrated circuits. It is also beneficial to use a material with the low dielectric constant (low-*K*) to fill the space between Cu interconnect lines in order to reduce the amount of cross talk between interconnects and place them closer to each other. Basically, it is the whole materials system that has been changed with the introduction of Cu metallization.

The difficulties of poor low-*K* dielectric materials and copper adhesion and diffusion into a silicon substrate have been challenging, but were overcome by Motorola, as well as other IC manufacturers. A thorough study is required to ensure the device reliability, which depends on many factors, including the ability of the device materials to withstand intrinsic stresses without falling apart.

For the above-mentioned mechanical reliability four materials properties are important, namely thin

*Corresponding author. Tel.: +1-480-413-3092; fax: +1-480-413-2656.
E-mail address: alex.volinsky@motorola.com (A.A. Volinsky).

0167-9317/03/$ – see front matter
doi:10.1016/S0167-9317(03)00341-1

film elastic modulus, yield stress, fracture toughness and adhesion. All these properties can be measured by means of nanoindentation.

2. Elastic modulus and hardness measurements

Thin film mechanical properties (elastic modulus and yield strength) can be measured by tensile testing of freestanding films [1] and by the microbeam cantilever deflection technique [2–4], but the easiest way is by means of nanoindentation. Here, no special sample preparation is required and tests can be performed quickly and inexpensively. Nanoindentation is similar to conventional hardness tests, but is performed on a much smaller scale using special equipment. The force required to press a sharp diamond indenter into tested material is recorded as a function of indentation depth.

Both elastic modulus and hardness can be readily extracted directly from the nanoindentation curve [5–8]. Since the depth resolution is on the order of nanometers, it is possible to indent even very thin (100 nm) films. A typical load–displacement curve of a 1 μm thick Cu film is shown in Fig. 1.

Elastic modulus is determined based on the knowledge of the tip shape function, A and the load–displacement curve (load P and displacement h) [6]:

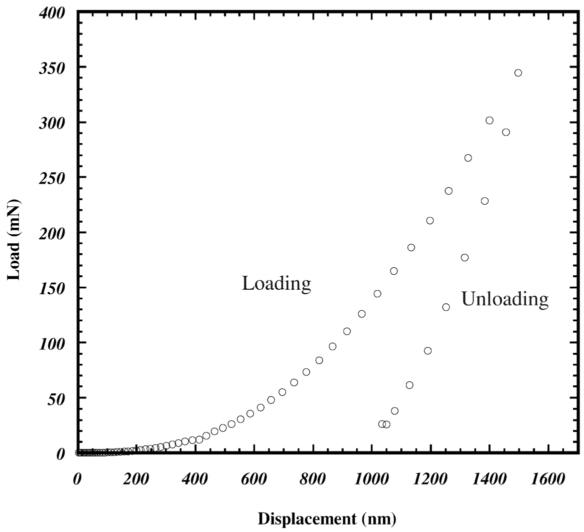

Fig. 1. Load–displacement curve for a 1 μm thick Cu film.

$$E_r = \frac{\sqrt{\pi}}{2} \cdot \frac{dP}{dh} \cdot \frac{1}{\sqrt{A}} \tag{1}$$

Here, dP/dh is taken for the unloading portion of the curve (Fig. 1), and E_r is the reduced modulus of the sample and the indenter material:

$$\frac{1}{E_r} = \frac{1-\nu_1^2}{E_1} + \frac{1-\nu_2^2}{E_2} \tag{2}$$

where ν_1 and ν_2, E_1 and E_2 are Poisson's ratios and elastic moduli of the film and the indenter material, respectively. Hardness is defined as the ratio of indentation load and projected contact area:

$$H = \frac{P_{max}}{A_{projected}} \tag{3}$$

For a metal film the yield stress, σ_{ys}, can be taken as the 1/3 of the hardness [9] measured by nanoindentation, or more accurately it can be extracted from the extent of the plastic zone size around the indenter, c, measured by atomic force microscopy (AFM), using Johnson's spherical cavity model approach [10]:

$$\sigma_{ys} = \frac{3P_{max}}{2\pi c^2} \tag{4}$$

where P_{max} is the maximum indentation load. Although this was originally applied for the bulk materials, it was also shown to be applicable in the case of thin films [11].

In the case of a metal thin film, the yield stress is typically much higher than for a bulk material. Since metal films are typically nanocrystalline, this is explained by the Hall–Petch type relationship between the film yield stress and its grain size, d:

$$\sigma_{ys} = \sigma_i + kd^{-n} \tag{5}$$

where σ_i is some intrinsic stress, independent of the grain size d, and n is typically between 0.5 and 1. The classic $1/d^{0.5}$ Hall–Petch relationship is not typically observed for thin films due to the substrate effect, limiting thin film plasticity, or due to the dislocation looping along the metal/oxide interface [12]. Similar effects are observed in different nanocrystalline bulk materials and thin films [13,14]. This should not be confused however with the bulk material surface preparation effects on the hardness [15].

If the grain size of a thin film scales with the film thickness, t, the film thickness can be used instead of the grain size as the scaling parameter [16]:

$$\sigma_{ys} = \alpha\left(1 + \beta t^{-1/2}\right) \tag{6}$$

where α and β are the fitting parameters. A similar approach, based on the film thickness is used by Nix [12] to predict Cu flow stress behavior.

Electroplated Cu grain size was obtained using both AFM and focused ion beam (FIB) imaging, and the yield stress was measured by nanoindentation, taking 1/3 of the hardness and also using Eq. (6) [11]. For electroplated annealed Cu films the following dependences of yield stress (in MPa) on grain size and the film thickness can be used (Fig. 2):

$$\sigma_{ys} = 180 + 0.262d^{-1/2} \quad \text{or}$$
$$\sigma_{ys} = 230 \cdot \left(1 + 0.577t^{-1/2}\right) \tag{7}$$

where d is the thin film grain size in microns, and t is the film thickness in microns.

As grain growth is typically observed in electroplated Cu films at room temperature (self-anneal process), thermal treatment is necessary, and may drastically affect thin film performance through altering microstructure. This includes both electromigration performance and the change in plasticity properties as depicted by Eq. (7). Plasticity of metal films greatly affects their adhesion performance as will be discussed in the next section.

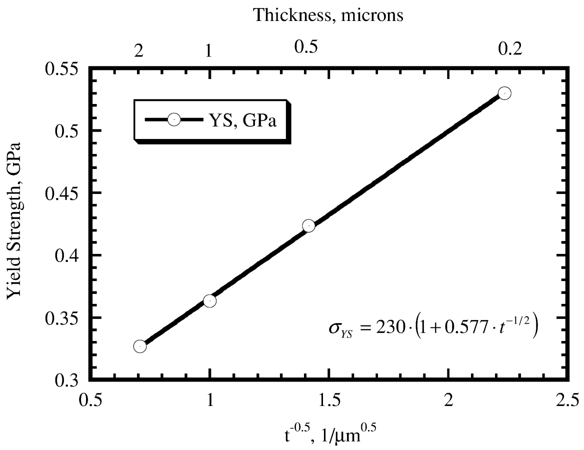

Fig. 2. Electroplated Cu yield stress.

Elastic modulus and hardness of different low-K materials were previously measured using nanoindentation [17–19], depending on the amount of porosity and composition, the elastic modulus of low-K dielectric films varied from 2 to 14 GPa, and the hardness varied from 0.5 to 2 GPa. A linear relationship between the elastic modulus and hardness was found for the silicate low-K dielectric films [17–19] (Fig. 3) when using Oliver and Phar analysis or continuous stiffness measurement (CSM) approach with sharp Berkovich indenters. As the mechanical response of low-K dielectric films is quite different from metallic films, in a way that the former exhibit almost no plasticity (Fig. 4), it may be appropriate to use Hertzian analysis with spherical tips for extracting elastic properties.

To first order the tip function for projected contact area, A, is related to the indentation depth, h, as $A = 24.5h^2$, so we can write:

$$H = \frac{P_{max}}{24.5h_{max}^2} \quad \text{and} \quad E_r = \frac{\sqrt{\pi}}{2} \cdot \frac{dP}{dh} \cdot \frac{1}{\sqrt{24.5}h} \tag{8}$$

This assumes a perfectly sharp tip and for tips with finite radius of curvature, a simple correction can be made [20]. The load–displacement curve does not exhibit much of a hysteresis between the loading and unloading (Fig. 4). This suggests that the contact is mostly elastic, and plasticity in these films is limited at least in the tested range of indentation depth. Even though the indentation depth is well beyond a spherical shape for this sharp Berkovich tip, we note that the observed elastic behavior follows the power law, where $P \sim h^{3/2}$ (Fig. 5). Thus, it appears that for both loading and unloading portions of the curve load is proportional to $h^{3/2}$. If the unloading stiffness then can be treated as Sneddon's for a circular punch [21], one would get:

$$E_r = \frac{\sqrt{\pi}}{2} \cdot \frac{dP}{dh} \cdot \frac{1}{\sqrt{24.5}h} = \text{const} \cdot \frac{dP}{dh} \cdot \frac{1}{h} = \frac{\text{const}}{\sqrt{h}} \tag{9}$$

Taking hardness as $H = P/(const \cdot h^2) = const/\sqrt{h}$, we see that the resulting ratio $E/H =$ constant for the load–displacement profiles following the elastic $P\sim$

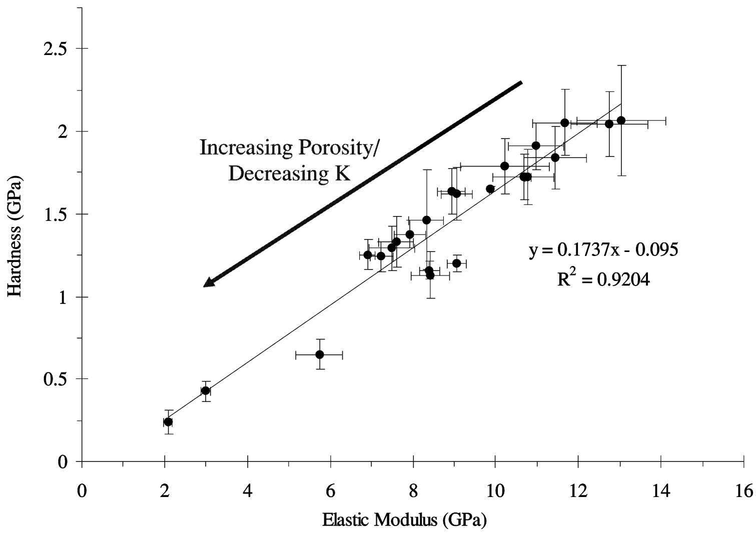

Fig. 3. Linear relationship between the hardness and the elastic modulus of low-*K* dielectric thin films.

$h^{3/2}$ law. This however arrives at the unacceptable result that the modulus is a function of the indentation depth. Typically there is an increase in the measured elastic modulus at the film surface originally attributed to the difficulty of determining the point of contact and the tip function at shallow depth (Fig. 6). At greater depth the modulus reaches the minima, and then the tip starts feeling the presence of a higher modulus substrate, so the measured modulus increases. It turns out that in addition to the surface effects, one would have to consider the modulus decrease with indentation depth as depicted by Eq. (9), and Sneddon's analysis might not be appropriate for the films exhibiting elastic $P \sim h^{3/2}$ behavior.

When almost elastic contact is observed using a Berkovich tip with materials exhibiting little or no plasticity, such as low-*K* dielectrics in this case, one can use a spherical tip with Hertzian analysis [22]. For elastic Hertzian contact indentation load is related to the indentation depth as:

$$P = \frac{4}{3} \cdot E_r \sqrt{Rh^3} \quad (10)$$

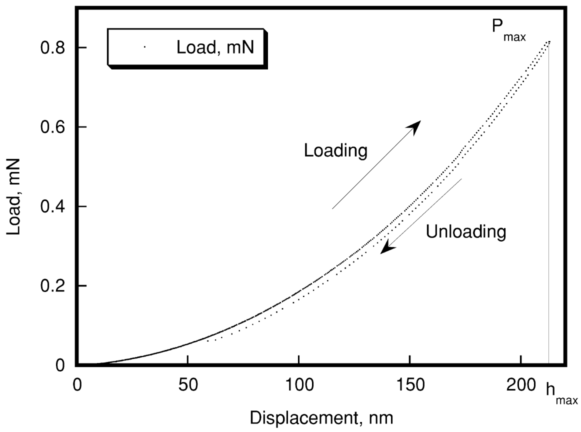

Fig. 4. Load–displacement curve for a 1 μm thick low-*K* dielectric film.

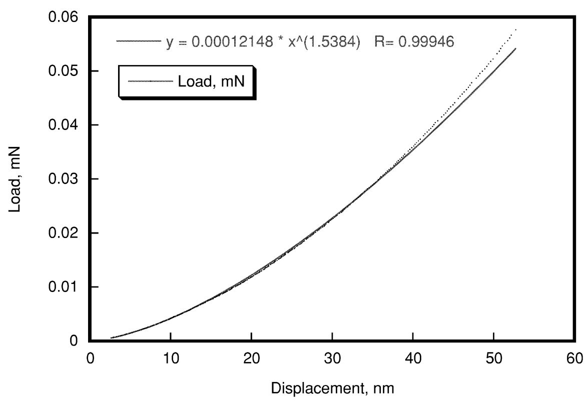

Fig. 5. Fit of a 3/2 power law fit to the elastic portion of the load–displacement data from Fig. 4.

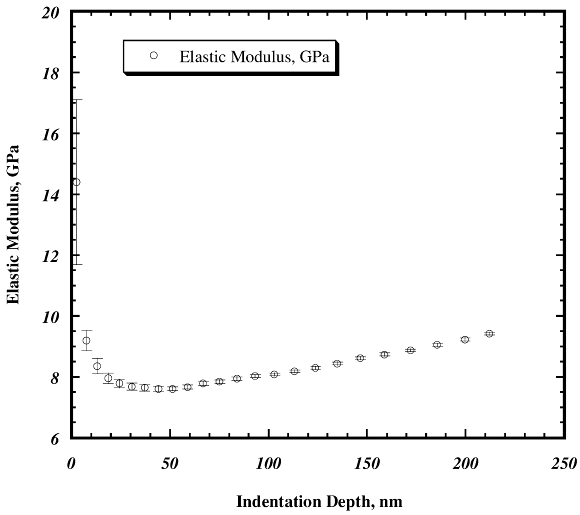

Fig. 6. Elastic modulus (measured using continuous stiffness measurement) as a function of indentation depth.

Now the reduced film modulus can be readily extracted from Eq. (10) if the spherical tip radius, R is known and the loading and unloading curves are elastic as in Fig. 4. In conclusion it should be pointed out that low-K materials are quite porous. Porosity effects on the mechanical properties of low-K dielectrics are discussed in Refs. [17,19,23].

3. Thin film adhesion measurements

Indentation has been also used to measure thin film adhesion [24–27], where the mechanical energy release rate, or practical work of adhesion is calculated based on the size of delamination that can be generated by high load (200–800 mN) indentation. For the most well adhered and ductile films a highly stressed superlayer needs to be deposited on top of the tested film. Deposition of a hard film, capable of storing sufficient amounts of elastic energy over the film of interest, can result in multilayer debonding [28], producing larger delamination radii. It also acts like a capping layer, preventing plastic flow of the underlying film in the vertical direction, adding normal stresses at the interfacial crack tip [25–27]. For the superlayer indentation test a sharp indenter also provides additional stress for crack initiation/propagation at the interface. A superlayer test

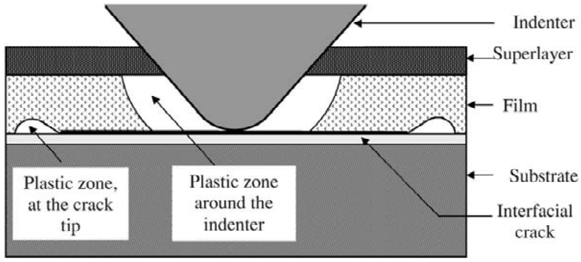

Fig. 7. Superlayer indentation test schematic (after Fig. 2 in Ref. [26]).

schematic is presented in Fig. 7. There would always be a plastic zone size around the indenter, and, depending on the testing material, ahead of the interfacial crack tip. It is important to make sure that those plastic zones do not overlap. Typically, the delamination radius has to be at least three to five times larger than the indenter contact radius in order to avoid this phenomena, also called the tip interaction effect [23,27]. The practical work of adhesion is calculated based on the Marshall and Evans analysis [24]:

$$\frac{GE_{\mathrm{f}}}{(1-\nu_{\mathrm{f}})} = \frac{1}{2}\cdot t\sigma_{\mathrm{I}}^{2}(1+\nu_{\mathrm{f}}) + (1-\alpha)(t\sigma_{\mathrm{R}}^{2}) - (1-\alpha)t(\sigma_{\mathrm{I}}-\sigma_{\mathrm{B}})^{2} \tag{11}$$

where E_{f} and ν_{f} are the thin film's Young's modulus and Poisson ratio, respectively, t is the film thickness, σ_{R} is the residual stress in the film, σ_{I} is the indentation stress from the indenter, σ_{B} is the Euler buckling stress of the film stack. The term α is equal to one if the film is not buckled, otherwise it represents the slope of the buckling load versus the edge displacement on buckling: $\alpha = 1 - [1/\{1 + 0.902(1-\nu_{\mathrm{f}})\}]$. Kriese and Gerebrich have modified this analysis and employed the laminate theory in order to calculate the necessary terms in Eq. (11) for the bilayer [25]. In the case of a highly compressed superlayer, the indentation stress is being added to the residual stress, so multiple superlayer depositions are avoided. Blanket films can be tested in the as-deposited, as-processed conditions; no pattern transfer is necessary. When an indenter penetrates through a bilayer, it causes film debonding and blister formation, which can be seen afterwards in an optical microscope with Nomarski contrast (Fig. 8).

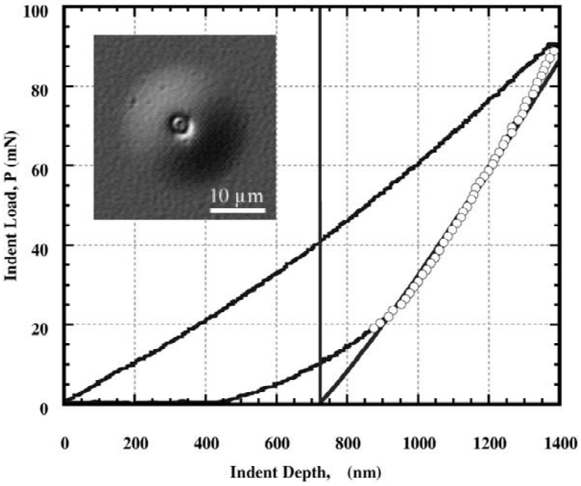

Fig. 8. Load–displacement curve and corresponding delamination of a W/Cu film stack.

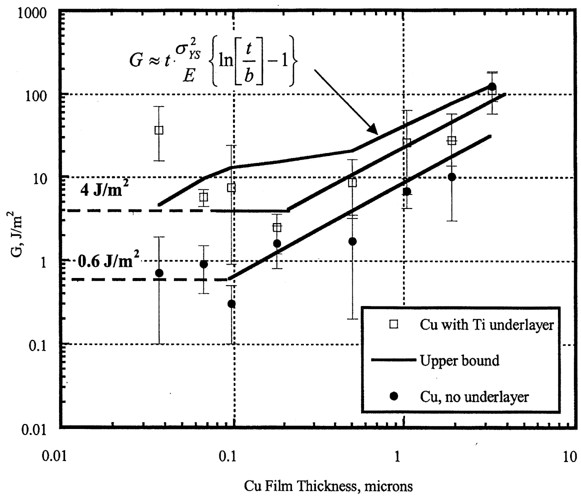

Fig. 9. Cu film practical work of adhesion as a function of film thickness (after Fig. 8 in Ref. [26]).

Properties of the films such as elastic modulus, Poisson's ratio, as well as the tip angle and radius are needed for an adhesion assessment. Generally speaking, there are two measurements that are necessary for strain energy release rate calculations. From the standpoint of blister formation, both indentation depth, h, and blister diameter, a, are required. Blister diameter is measured in the optical microscope with Nomarski contrast. Using the Oliver–Pharr method [8], inelastic indentation depth, h_{pl}, is calculated from:

$$P = \alpha(h - h_{pl})^{\beta} \tag{12}$$

where P and h are the load and displacement from the 65% of the unloading slope of the load–displacement curve, respectively (Fig. 8), α and β are fitting parameters. The indentation volume, V_I, is calculated from the inelastic depth by using the tip geometry. The indentation stress can be calculated as in [24]:

$$\sigma_I = \frac{V_I E_f}{2\pi t a^2 (1 - \nu_f)} \tag{13}$$

assuming the conservation of volume.

Fig. 9 shows the practical work of adhesion for a Cu film as a function of film thickness. The data presented is for Cu films deposited on SiO_2 and Ti layers on top of Si. As previously discussed in [26–31], there is a plastic energy contribution to the practical work of adhesion that increases with the film thickness over a 100 nm. Below a 100 nm film thickness almost no plasticity effects are observed, and the measured work of adhesion is approaching the thermodynamic work of adhesion of 0.6 and 4 J/m^2 for the Cu/SiO_2 and Cu/Ti interfaces, respectively. A simple plastic strip model [26] can be used as an upper bound for predicting practical work of adhesion of a metal thin film:

$$G \approx t \cdot \frac{\sigma_{ys}^2}{E} \cdot \left\{ \ln\left[\frac{t}{b}\right] - 1 \right\} \tag{14}$$

where t is the film thickness, and b is the Burgers vector. More advanced models can be found in Refs. [26,31].

Attempts have been made to measure the adhesion of low-K dielectric films to various substrates [18,19], and varied from 0.1 to 4.5 J/m^2. However, ex-situ FIB cross-sectioning of the delamination blisters showed that in most cases fracture occurred in the low-K dielectric layer itself. This phenomenon occurs since the interfacial fracture toughness (or adhesion) of the low-K/substrate interface exceeds the fracture toughness of the low-K material itself [18,19]. Fracture toughness is an important property to measure for the low-K dielectrics along with the interfacial adhesion.

4. Thin film fracture toughness measurements

Fracture toughness of a bulk brittle material can be calculated within 40% accuracy based on the maximum indentation depth, $P_{\max}$ and the crack length, a [32,33]:

$$K_C = \beta \cdot \left(\frac{E}{H}\right)^{1/2} \cdot \left(\frac{P_{\max}}{a^{3/2}}\right) \tag{15}$$

where β is an empirical constant which depends on the geometry of the indenter, and is 0.0319 for a cube corner indenter geometry [32,33], E is the elastic modulus, and H is the mean hardness. Although, technically speaking, any type of pyramid can induce radial cracks, it was shown that the cube-corner indenter provides a lower cracking threshold in terms of the maximum indentation load [33].

Fig. 10 represents three different scenarios one may observe using pyramid indentation. Fig. 10a is the desired configuration for radial cracks emanating from the corners of an indent. Due to the high shear stresses induced by the indenter pyramid edges subsurface delamination cracks are also observed for some indents (Fig. 10b and c). Similar fracture patterns have been observed in low-K films [18]. Lawn and Wilshaw [34] provide a detailed review of the indentation-induced cracking in brittle materials.

Eq. (15) should not be directly applied in the case of a thin film, since typically the crack shape is no longer halfpenny shape. An appropriate model should account for at least the film thickness and stress, and, preferably for the film porosity. Recent theoretical and experimental developments address this problem [16,17,34,35].

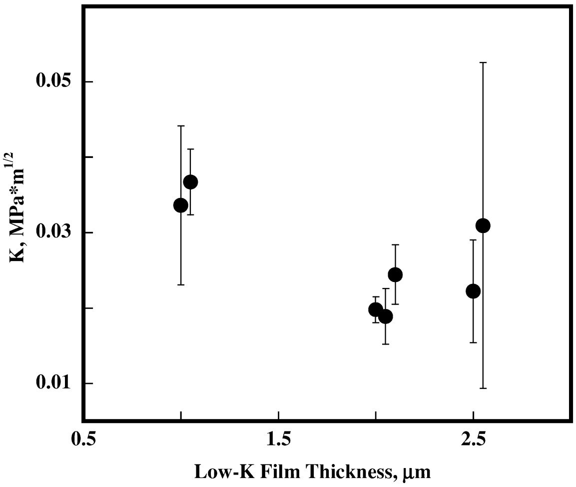

Fig. 11. Measured low-K film fracture toughness compared to the K values just due to the low-K film residual stress.

For a certain film thickness/load combination there is a linear dependence between the maximum indentation load and the radial crack length to the 1.5 power, $a^{3/2}$ [10]. With certain reservations Eq. (15) can be used to estimate fracture toughness of thin films (Fig. 11). In our previous studies [17,18] it was found that low-K dielectrics deposited on appropriate barrier layers are susceptible to cohesive, rather than interfacial fracture. Indentation fracture toughness measurements also agreed with the superlayer indentation test results, where cohesive low-K fracture was observed, and with an upper bound estimates

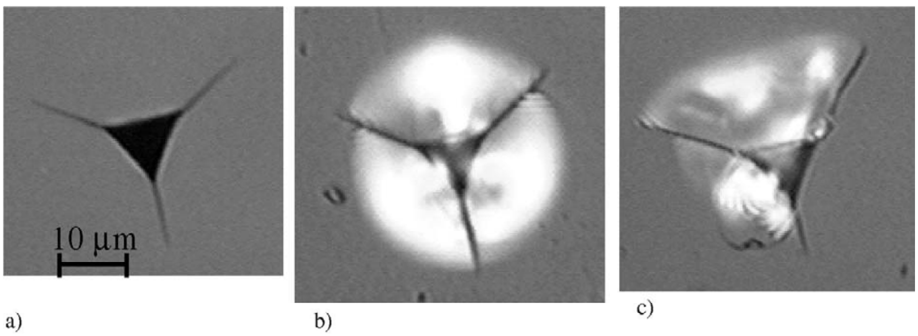

Fig. 10. Optical micrographs of cube-corner indentation-induced fracture in fused silica: (a) radial cracks; (b) radial as well as symmetric sub-surface cracks; (c) radial and asymmetric sub-surface cracks (after Fig. 10 in Ref. [18]).

based on the fact that some films fractured upon superlayer deposition [18].

Low-*K* film cracking has also been observed due to the relief of residual stress at a critical film thickness, on the order of 3 μm (Fig. 12). This can be used as another method of estimating the film fracture toughness. The low-*K* dielectric film tensile residual stress is approaching 44 MPa starting from the 0.5 μm film thickness [19], so one can estimate the strain energy release rate, *G* for this material following Hutchinson and Suo [36] analysis:

$$G = Z \cdot \frac{(1-\nu_f^2)\sigma_R^2 t}{E_f} \tag{16}$$

where σ_R is the residual stress, t is the film thickness, and E_f is the film elastic modulus, and Z is ranging from 1/2 to 4, depending on the sample geometry and the residual stress sign. In the case of 44 MPa tensile residual stress ($Z=1/2$) for a 3 μm critical film thickness, one would get 0.581 J/m^2 energy release rate, corresponding to about 0.054 MPa m$^{1/2}$. A simple analysis like this can provide realistic upper estimates of the thin film adhesion/toughness. Based on the knowledge of the residual stress and the film thickness, one can come up with a fracture criterion just due to the residual stress [18]:

$$K_C \leq \sigma_R \sqrt{Zt} \tag{17}$$

Eq. (17) is similar to a definition of *K*, except here the film thickness is used instead of the flaw size, or the crack length [37].

It is also important to remember that most of the mechanical properties change with temperature. With certain hardware modifications nanoindentation can be suited for measurements at higher temperatures, which is currently being investigated.

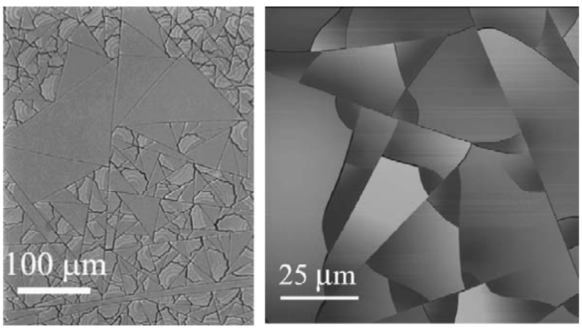

Fig. 12. Optical and AFM images (1 μm Z range) of a 3 μm thick low-*K* film cracking due to residual stress relief.

5. Conclusions

Nanoindentation is a powerful technique that can be applied in modern microelectronics for measuring thin film mechanical properties. While measuring elastic and plastic properties with nanoindentation is almost routine, and there are several commercial tools and software packages available, adhesion and fracture toughness measurements are still in the development stage. They require support of other characterization techniques, but can be adapted for production quality control applications.

6. Nomenclature

Unless otherwise specified, the following nomenclature is used in the paper:

A	Projected contact area
a	Crack length
α, β	Fitting parameters
b	Burger's vector
c	Plastic zone size
d	Grain size
E	Young's modulus
E_r	Reduced Young's modulus
G	Strain energy release rate
h	Indentation depth (displacement)
H	Hardness
K	Stress intensity at a crack tip
K_C	Critical stress intensity of a material
ν	Poisson's ratio
P	Load
R	Indenter tip radius
σ	Stress (σ_I, σ_B, σ_R are used for the indentation, buckling and residual stresses, respectively)
σ_{ys}	Thin film yield stress
t	Film thickness
V_I	Indentation volume

Acknowledgements

The authors would like to thank Dr. Neville R. Moody from Sandia National Laboratory for his support for this research. Great thanks to Joseph B. Vella for experiments with low-*K* and Cu mechanical properties measurements, and to Xiang-Dong Wang and Epiphany A. Irwing for AFM fracture analysis.

References

[1] D.T. Read, J.W. Dally, J. Mater. Res. 8 (7) (1993) 1542.
[2] T.P. Weihs, S. Hong, J.C. Bravman, W.D. Nix, J. Mater. Res. 3 (5) (1998) 931.
[3] S.P. Baker, W. D Nix, J. Mater. Res. 9 (12) (1994) 3131.
[4] S.P. Baker, W.D. Nix, J. Mater. Res. 9 (12) (1994) 3145.
[5] G.M. Pharr, D.S. Harding, W.C. Oliver, in: M. Nastasi et al. (Ed.), Mechanical Properties and Deformation Behavior of Materials Having Ultra-Fine Microstructures, Kluwer, Dordrecht, 1993, pp. 449–461.
[6] M. Doerner, W.D. Nix, J. Mater. Res. 1 (1986) 601.
[7] G.M. Pharr, W.C. Oliver, F. Brotzen, J. Mater. Res. 7 (3) (1992) 613.
[8] W.C. Oliver, G.M. Pharr, J. Mater. Res. 7 (1992) 1564.
[9] D. Tabor, in: The Hardness of Metals, Claredon Press, 1951, p. 174.
[10] D. Kramer, H. Huang, M. Kriese, J. Robach, J. Nelson, A. Wright, D. Bahr, W.W. Gerberich, Acta Mater. 47 (1999) 333.
[11] A.A. Volinsky, J. Vella, I.S. Adhihetty, V. Sarihan, L. Mercado, B.H. Yeung, W.W. Gerberich, Mater. Res. Soc. Symp. Proc. 649 (2000).
[12] W.D. Nix, Metall. Trans. A 20A (1989) 2217–2245.
[13] J.B. Savader, M.R. Scanlon, R.C. Camarata, D.T. Smith, C. Hayzelden, Scripta Mater. 36 (1) (1997) 29–34.
[14] L. Lu, L.B. Wang, B.Z. Ding, K. Lu, J. Mater. Res. 15 (2) (2000) 270–273.
[15] Y. Liu, A.H.W. Ngan, Scripta Mater. 44 (2001) 237–241.
[16] Y. Wei, J.W. Hutchinson, J. Mech. Phys. Solids 45 (7) (1997) 1137–1159.
[17] J.B. Vella, Q. Xie, N.V. Edwards, J. Kulik, K. Junker, in: C.S. Ozkan, L.B. Freund, R.C. Cammarata, H. Gao (Eds.), Thin Films—Stresses and Mechanical Properties IX, Boston, MA, 26–30 November 2001, Materials Research Society Proceedings, Vol. 695, 2001, p. L6.25.
[18] A.A. Volinsky, J.B. Vella, W.W. Gerberich, Thin Solid Films, 2002, in press.
[19] J.B. Vella, I.S. Adhihetty, K. Junker, A.A. Volinsky, Int. J. Fracture, 2002, in press.
[20] D.F. Bahr, J.W. Hoehn, N.R. Moody, W.W. Gerberich, Acta Mater. 45 (No. 12) (1997) 5163–5175.
[21] I.N. Sneddon, Boussinesq's problem for a plat-ended cylinder, in: Proc. Cambridge Philosophical Society, Vol. 42, 1946, pp. 29–39.
[22] W.W. Gerberich, W. Yu, D. Kramer, A. Strojny, D. Bahr, E. Lilleodden, J. Nelson, J. Mater. Res. 13 (No 2) (1998) 421.
[23] A.A. Volinsky, M.-L.B. Palacio, W.W. Gerberich, in: Materials Research Society Proceedings, Vol. 750, 2002, p. Y9.9.
[24] D.B. Marshall, A.G. Evans, J. Appl. Phys. 56 (1984) 2632.
[25] M.D. Kriese, W.W. Gerberich, J. Mater. Res. 14 (7) (1999) 3007.
[26] A.A. Volinsky, N.I. Tymiak, M.D. Kriese, W.W. Gerberich, J.W. Hutchinson, Mater. Res. Soc. Symp. Proc. 539 (1999) 277.
[27] A.A. Volinsky, N.R. Moody, W.W. Gerberich, Acta Mater. 50/3 (2002) 441.
[28] A. Bagchi, A. Evans, Thin Solid Films 286 (1996) 203–212.
[29] N.I. Tymiak, A.A. Volinsky, M.D. Kriese, S.A. Downs, W.W. Gerberich, Metall. Mater. Trans. A 31A (No. 3A) (2000) 863–872A.
[30] M. Lane, R.H. Dauskardt, N. Krishna, I. Hashim, J. Mater. Res. 15 (1) (2000) 203–211.
[31] W.W. Gerberich, A.A. Volinsky, N.I. Tymiak, N.R. Moody, Mater. Res. Soc. Symp. Proc. 594 (2000).
[32] G.M. Pharr, D.S. Harding, W.C. Oliver, in: M. Nastasi et al. (Ed.), Mechanical Properties and Deformation Behavior of Materials Having Ultra-Fine Microstructures, Kluwer, Dordrecht, 1993, p. 449.
[33] D.S. Harding, W.C. Oliver, G. M Pharr, Mater. Res. Soc. Symp. Proc. 356 (1995) 663.
[34] B. Lawn, R. Winslaw, J. Mater. Sci. 10 (1975) 1049.
[35] R. Cook, D. Morris, University of Minnesota, MN, 2002, unpublished work.
[36] J. Hutchinson, Z. Suo, Adv. Appl. Mech. 29 (1992) 63.
[37] D.B. Marshall, B.R. Lawn, A.G. Evans, J. Am. Ceram. Soc. 65 (11) (1982) 561–566.